

# RSC Advances

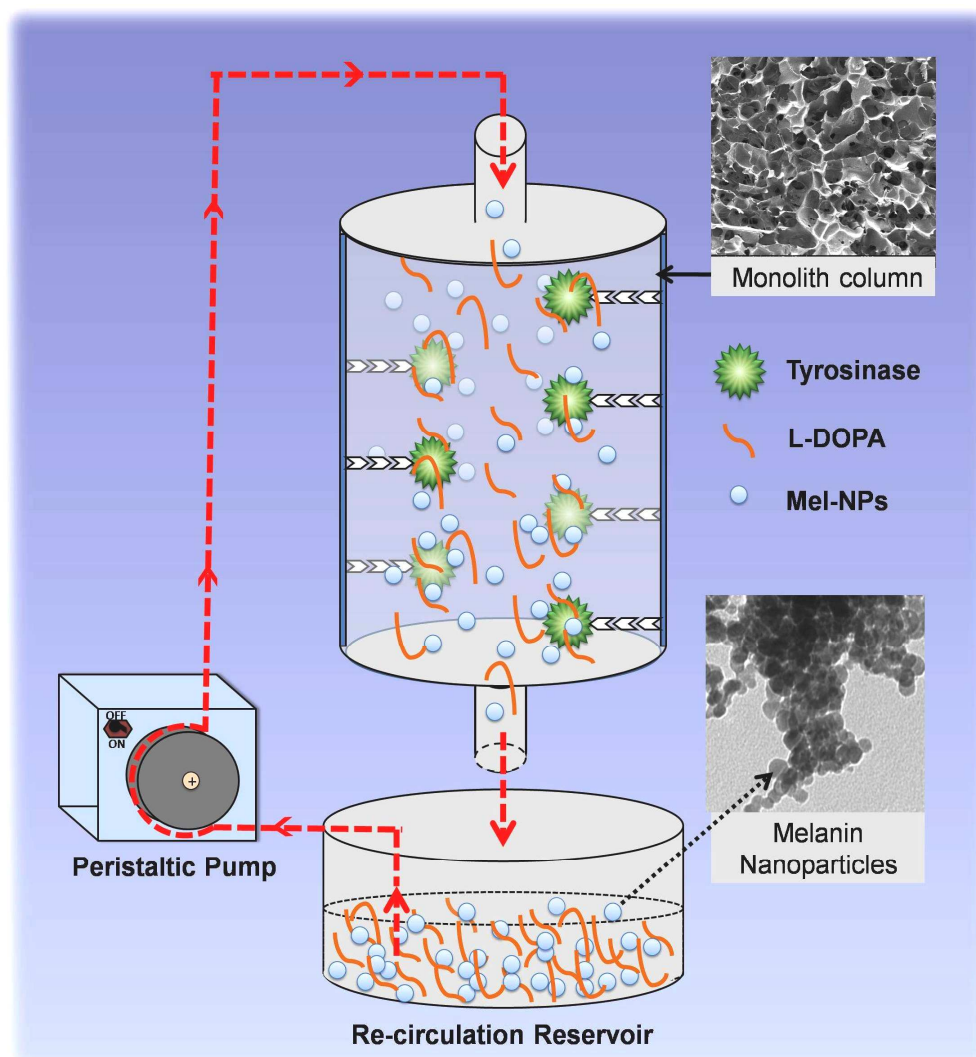


This is an *Accepted Manuscript*, which has been through the Royal Society of Chemistry peer review process and has been accepted for publication.

*Accepted Manuscripts* are published online shortly after acceptance, before technical editing, formatting and proof reading. Using this free service, authors can make their results available to the community, in citable form, before we publish the edited article. This *Accepted Manuscript* will be replaced by the edited, formatted and paginated article as soon as this is available.

You can find more information about *Accepted Manuscripts* in the [Information for Authors](#).

Please note that technical editing may introduce minor changes to the text and/or graphics, which may alter content. The journal's standard [Terms & Conditions](#) and the [Ethical guidelines](#) still apply. In no event shall the Royal Society of Chemistry be held responsible for any errors or omissions in this *Accepted Manuscript* or any consequences arising from the use of any information it contains.

**Graphical Abstract**

“Novel approach for biosynthesis of melanin nanoparticles by sequestrial biotransformation of L-DOPA using immobilized tyrosinase enzyme in macroporous poly(AAm-co-AGE) monolith”

# On-column enzymatic synthesis of melanin nanoparticles using cryogenic poly(AAM-co-AGE) monolith and its free radical scavenging and electro-catalytic properties

Amardeep Singh Saini, Anuj Tripathi, and Jose Savio Melo\*

Nuclear Agriculture and Biotechnology Division, Bhabha Atomic Research Centre, Mumbai- 400085, India

Author's Email: jsmelo@barc.gov.in (J.S. Melo), anujtri@barc.gov.in (A. Tripathi) and

saini\_amardeepsingh@yahoo.co.in (A.S. Saini)

\* Tel.: +91 22 25592760; Fax: +91 22 25505151

## Abstract

In the present study we have demonstrated a green-route for the synthesis of melanin nanoparticles (Mel-NPs). To achieve this, a monolith column of poly(acrylamide-co-allylglycidyl ether) was synthesized and further modified to immobilize the enzyme tyrosinase, which was extracted from the corm of plant tuber *Amorphophallus campanulatus*. The immobilization of the enzyme was carried out in two steps. First, the epoxy groups present on the monolith surface were coupled with ethylene diamine followed by glutaraldehyde to introduce aldehyde moieties. In the second step, aldehyde functionalized monolith column was treated with enzyme solution for covalent bonding through Schiff's base formation. The physico-chemical characterization of monolith, exhibited ideal column characteristics like interconnected pore architecture, high flow rate, hydrophilicity and amiable mechanical strength. The convective flow of L-3,4-dihydroxyphenylalanine through the column brought about its conversion to Mel-NPs by biocatalytic activity of the immobilized enzyme. The spectral changes of the solution recorded in UV-visible region at regular time intervals showed that the synthesis of Mel-NPs occurred via formation of different intermediates. The size of the spherical Mel-NPs was in the

range of 20 to 30 nm and its colloidal stability at different pH values was confirmed by measuring the zeta potential after a period of 8 weeks. FT-IR and TG analysis indicated that the bio-synthesized Mel-NPs showed characteristics similar to that of natural melanin. The  $IC_{50}$  value for free-radical scavenging activity of Mel-NPs was calculated to be  $24 \mu\text{g mL}^{-1}$  using DPPH assay. Ferric-reducing action of Mel-NPs showed a concentration dependent increase under experimental conditions. Further, electro-catalytic activity of the glassy carbon electrode (GCE) modified with Mel-NPs was evaluated and was found to show a 2.4 fold enhancement in electro-chemical signal when compared with bare electrode. In conclusion, Mel-NPs synthesized by this novel approach can find applications in the development of antioxidant formulations, biosensor and other areas of interest.

**Keywords:** Biosynthesis, melanin-nanoparticle, tyrosinase, macroporous, monolith

## 1. Introduction

In recent years, metallic nanoparticles have been the focus of research due to their unique properties that are attributed to their small size and large surface area.<sup>1</sup> For these reasons, nanoparticles have found applications in different fields such as biomedical, electrochemical, diagnostic imaging, etc.<sup>2</sup> More recently, nanosized organic particles are gaining interest in modern day scenario.<sup>3</sup> Organic nanoparticles have met a great expansion in the area of microelectronics, photonics<sup>4</sup> and also as chromophoric colloids with special demand in coloring of drinks and foodstuff.<sup>5</sup>

Melanin is a broad class of natural pigment which is emerging as a powerful natural organic compound that has profound interdisciplinary applications. Research on melanin has revealed a variety of biological functions. For example, the most important function of melanin in human body is to act as a photoprotectant. Also, melanin has attracted attention because of its interesting properties such as an antioxidant,<sup>6</sup> radioprotectant,<sup>7</sup> in cancer treatment,<sup>8</sup> in immunomodulation,<sup>9</sup> and as a potential cytokine regulator.<sup>10</sup> The importance of melanin has also been discussed as an adsorbent for drug residues<sup>11</sup> and in AIDS treatment.<sup>12</sup> Sunscreens containing melanin can protect against harmful U.V. radiation which can cause melanoma and other cancers of the skin.<sup>13</sup>

Melanin has also been shown to be important in several non-biological applications. It shows various physico-chemical properties including broad band absorbance, extremely low radiative quantum yield and condensed phase photo-conductivity<sup>14</sup> due to which it can be used as bio-inspired high-tech material in applications such as bioelectronics,<sup>15</sup> chemical sensing<sup>14</sup> and photon detection.<sup>16</sup> Turick *et al*, have shown that gamma radiation can interact with melanin to alter its oxidation-reduction potential and result in generation of electric current.<sup>17</sup>

Melanin is a nearly ubiquitous pigment in biology. It can be isolated from various natural sources.<sup>18-22</sup> Most of the melanin that is isolated from natural sources is not easily dispersed in water, restricting its efficacy for potential application. Therefore, it is important to develop a new method for synthesis of Mel-NPs with good colloidal dispersion in aqueous solution. A few studies have already demonstrated the synthesis of melanin or melanin like nanoparticles.<sup>18,23-26</sup> However, these studies have involved the chemical route for synthesis of melanin nanoparticles, which may pose environmental concerns. Therefore, the biological approach for synthesis of melanin nanoparticles gains importance.

Biological methods for the synthesis of different nanoparticles using biomolecules, bacteria, yeast, fungus and plant or their extracts are an eco-friendly alternative to the chemical methods.<sup>27</sup> Using enzymes as biocatalysts offers numerous advantages such as selectivity, specificity, mild reaction conditions and an environment friendly process.<sup>28</sup> Tyrosinase is the key enzyme involved in the synthesis of melanin pigment.<sup>29,30</sup> It catalyzes the oxidation of L-Dopa to give an intermediate product “quinone” that later polymerizes and gives rise to the black color melanin pigment. Tyrosinase enzyme can be obtained from a variety of sources namely bacteria, fungi, and plants. Our group has shown the use of tyrosinase from plant, *Amorphophallus campanulatus* for application in biosensor.<sup>31</sup> Moreover, from our recent study, it was observed that free form of tyrosinase enzyme catalyses the biotransformation of L-Dopa to melanin.<sup>32</sup> However, the process involves uncontrolled interaction of enzyme with substrate followed by agglomeration and melanin thus obtained was in micron size range. Also, the use of free enzyme suffers from various limitations such as reusability, stability, product inhibition and contamination, besides cost factor. In order to overcome these limitations, immobilization of enzyme can play a major role.<sup>33-36</sup> During the process of immobilization, the enzyme needs to be

properly oriented along with the help of a spacer arm to interact with large substrates.<sup>37</sup> Further, multipoint attachment of enzyme to the support makes it less sensitive to conformational changes under drastic conditions in comparison to free enzyme.<sup>38</sup> Immobilization can also improve the kinetic properties of the enzyme depending on the micro-environment generated around the enzyme.<sup>39</sup> However, there is no universal method of enzyme immobilization and depending on the requirement, the technique needs to be devised.

Previous studies have demonstrated the potential of on-column enzyme/cells immobilization for efficient bioprocess applications and control of reaction.<sup>40-42</sup> Such results have encouraged us to synthesize Mel-NPs using immobilized enzyme on a column. In the recent past, various immobilization approaches have been developed. Among these, porous matrices are gaining interest as one of the attractive system for immobilization.<sup>43,44</sup> Porous matrices provide amiable surface area with the possibility for modification with desired ligands for stable immobilization of functional biomolecules. Additionally, an ideal immobilization carrier should have structural strength, low hydraulic resistance with suitable diffusive properties and should be stable to temperature, pH and ionic strength.<sup>45</sup> Monolith design is an efficient format which provides high porosity to the column and eventually provides high surface area for large molecular reactivity. Hence, large void volume availability reduces the back pressure and diffusion of analyte through the pore channels in monolith. Thus, if the final product is a nanoparticle, using monolith could prevent the problems that might be expected while using conventional porous supports. Considering these advantages, a porous polymeric monolith would be a suitable choice for immobilizing the enzyme and then use for biotransformation.

In this context, we report the development of a novel bioprocess for the synthesis of Mel-NPs through green chemistry route. A porous polymeric poly(acrylamide-co-allylglycidyl ether)

monolith column was synthesized and surface modified for the immobilization of tyrosinase enzyme from *A. campanulatus*. Synthesis of Mel-NPs in the monolith column was studied by following the conversion of 3,4-dihydroxyphenylalanine (L-Dopa) under continuous flow. Further, the biosynthesized Mel-NPs were characterized using different analytical techniques such as UV-visible spectroscopy, TEM, zeta potential measurement, FT-IR and thermogravimetric analysis (TGA). The free-radical scavenging and electro-catalytic activity of Mel-NPs were investigated for its biological applications.

## 2. Experimental

### 2.1. Materials

Acrylamide (AAm,  $\geq 99\%$ ), *N,N'*-methylene-bis(acrylamide) (MBAAm, 99%), allylglycidyl ether (AGE,  $\geq 99\%$ ), glutaraldehyde solution (25% in H<sub>2</sub>O), ammonium persulfate (APS,  $\geq 98\%$ ), *N,N,N',N'*-tetra-methylethylenediamine (TEMED,  $\sim 99\%$ ), sodium borohydride (NaBH<sub>4</sub>,  $\geq 98\%$ ), polyethyleneimine (PEI, 50% w/v in H<sub>2</sub>O), 3,4-dihydroxyphenylalanine (L-Dopa;  $\geq 98\%$ ) and 2,2-diphenyl-1-picryl-hydrazyl (DPPH; M.W.-394.32), were purchased from Sigma-Aldrich, Germany. 1,2-diaminoethane (99%) was obtained from Sisco Research Laboratories (SRL) (Mumbai, India). Tyrosinase enzyme was extracted from corm of the tuber *A. campanulatus* which was purchased from the local market. Ultrapure water with a specific resistance of 18.2 M $\Omega$ -cm was used for all experimental preparations (Elix<sup>®</sup> Millipore). Glassy carbon electrode (GCE) was purchased from CH Instruments Company (Shanghai, China). All the other reagents used were of analytical grade.

### 2.2. Extraction of tyrosinase enzyme from *A. campanulatus*

Tyrosinase was extracted from corm of the tuber *A. campanulatus* and then subjected to partial purification.<sup>31</sup> Briefly, *A. campanulatus* (1 kg) was homogenized using chilled phosphate buffer

(0.1 M, pH 6) and filtered using cheese cloth. This filtrate was centrifuged (2500 rpm for 7 min, 4 °C) and the supernatant was further subjected to ammonium sulfate precipitation (60% saturation) under cold conditions. The precipitate obtained was further re-dissolved in fresh extraction buffer and dialyzed against ultrapure water. The sample was then assayed for total protein content by Folin's Lowry method and the tyrosinase activity was calculated by measuring the formation of dopachrome ( $\lambda_{\text{max}} = 475 \text{ nm}$ ,  $\epsilon = 3700 \text{ M}^{-1} \text{ cm}^{-1}$ ). One unit of enzyme activity was defined as increase in absorbance by 0.001 per minute at 475 nm at pH 6.0 and temperature of 30 °C. Extracted enzyme had 1.6 mg mL<sup>-1</sup> of protein content and 7500 U mg<sup>-1</sup> of specific activity.

### **2.3. Synthesis of poly(acrylamide-co-allylglycidyl ether) porous monolith column and its physical properties**

Polymeric macroporous poly(acrylamide-co-allylglycidyl ether) (poly(AAm-co-AGE)) monolith column was synthesized as per the procedure described by Arvidsson *et al*<sup>46</sup> (see supplementary S1.1). For the present study, monolith column of 6% poly(AAm-co-AGE) was synthesized in a plastic syringe (Becton Dickinson, India) (20 mm height × 8 mm diameter). After incubation at subzero temperature, a polymeric monolith of poly(AAm-co-AGE) was obtained by thawing of water at room temperature (25 ± 2 °C). The poly(AAm-co-AGE) monolith column was then thoroughly washed with ultrapure water and dried at room temperature for further use. Poly(AAm-co-AGE) monolith matrix was morphologically examined by scanning electron microscopy (SEM). The physical properties like water uptake kinetics, swelling ratio, porosity, flow rate, hydraulic permeability and rheology of monolith were performed as per the standard procedures,<sup>47</sup> which are described in supplementary data (S1.2).

#### 2.4. Functionalization of poly(AAm-co-AGE) monolith for immobilization of tyrosinase

Water saturated monolith of poly(AAm-co-AGE) (20 mm height  $\times$  8 mm diameter) was placed in the syringe with same diameter and 10 mL of 0.5 M Na<sub>2</sub>CO<sub>3</sub> solution was passed through the syringe column at a flow rate of 1 mL min<sup>-1</sup> for activating the epoxy groups. Then, 1,2-diaminoethane (0.5 M in 0.5 M Na<sub>2</sub>CO<sub>3</sub>, pH  $\geq$ 10) was circulated through the monolith column at a flow rate of 1 mL min<sup>-1</sup> for 24 h at room temperature. The amino group functionalized column was then washed with de-ionized water until the pH dropped to 7. Further, column was treated with glutaraldehyde solution (0.2% v/v in 0.1M phosphate buffer, pH 6) for 4 h in a circulating mode followed by washing with three column volumes of phosphate buffer (pH 6). The *A. campanulatus* derived tyrosinase enzyme (12000 U of enzyme solution prepared in 5 mL of 0.1M phosphate buffer, pH 6) was circulated through the monolith column at 4 °C overnight in the dark. Further, the freshly prepared NaBH<sub>4</sub> solution (0.1 M in sodium carbonate buffer, pH 9.2; 30 ml) was used to reduce Schiff's base formed between the enzyme and the aldehyde. Finally, this enzyme functionalized porous monolith column was equilibrated with phosphate buffer (0.1 M, pH 6) and kept at 4 °C for further use.

#### 2.5. Biosynthesis of Mel-NPs

For the synthesis of Mel-NPs, L-Dopa (5 mM) was dissolved in ultrapure water (50 mL) at 30 °C. This solution was then circulated through the tyrosinase immobilized monolith column for 24 h at a flow rate of 60 mL h<sup>-1</sup>. The bioconversion of L-Dopa to melanin was monitored by inspecting the visual change in the color of solution during the biocatalysis as well as by measuring the change in absorbance of the circulated solution at regular time intervals. UV-visible absorbance spectrum of the synthesized Mel-NPs was monitored using Jasco V-530 UV-visible double beam spectrometer in the wavelength range of 325-700 nm. The absorbance of the

solution was measured at  $25 \pm 2$  °C in a quartz cuvette with an optical path of 1 cm. After completion of the reaction, the solution was subjected to dialysis against ultrapure water to remove any un-reacted substrate. The dialyzed solution was lyophilized and the powder thus obtained was stored at 4 °C for further characterization. For reproducibility, the experiments were repeated five times under similar conditions.

## 2.6. Characterization of biosynthesized Mel-NPs

Microscopic examination of Mel-NPs was performed using transmission electron microscope (TEM) (Carl Zeiss Libra 120, Germany) with an accelerating voltage of 120 kV. However, Mel-NPs were stained with  $100 \text{ mg L}^{-1}$  of uranyl nitrate hexahydrate (Merck, Germany, > 98%) solution prior to TEM analysis for improving the imaging of low density organic matter. Then, Mel-NPs were placed on a carbon coated copper grid (Ted Pella, Inc.) and dried before observing under the microscope. The measurement of zeta potential was performed for analyzing the surface charge behavior of Mel-NPs with respect to pH. Different sets of Mel-NPs ( $1 \text{ mg mL}^{-1}$ ) were suspended in de-ionized water. Further, pH was adjusted from 2 to 11 with the help of 1 N HCl and 1 N NaOH without addition of background electrolytes. These samples were incubated for 8 weeks at room temperature ( $25 \pm 2$  °C) followed by zeta potential ( $\zeta$ ) analysis using a Zetasizer analyzer (Nano-Z series, Malvern, UK). FT-IR spectra of Mel-NPs were recorded using FT-IR-660 plus infrared spectrometer (Jasco, Japan). For measurement, dried powder of Mel-NPs was mixed with KBr powder (IR grade) in the ratio of 1:10 (w/w), respectively, and ground until a uniform color of mixture was achieved. The spectrum was recorded over a range from  $4000 \text{ cm}^{-1}$  to  $400 \text{ cm}^{-1}$  with a resolution of  $4 \text{ cm}^{-1}$ . Thermogravimetric analysis (TGA) of the Mel-NPs was performed under nitrogen atmosphere from 0 to 1000 °C at

a heating increment of 10 °C min<sup>-1</sup> in an inert atmosphere for understanding the thermal behaviour and stability.

## 2.7. Free radical scavenging property of Mel-NPs

The free radical scavenging property of Mel-NPs was studied using DPPH assay. For this, DPPH solution (0.1 mM) was freshly prepared in methanol before carrying out the experiments. To 1 mL of DPPH solution, 200 µL of varying concentrations of Mel-NPs (50 to 500 µg mL<sup>-1</sup>) were added. The final Mel-NPs concentration in the reaction mixture ranged from 8.3 to 83.3 µg mL<sup>-1</sup>. This mixture was then kept at room temperature under dark conditions for 20 min. After incubation, the absorbance of the solution was measured at 517 nm against a blank. The ability to scavenge DPPH radicals was calculated using the following equation:

$$\% \text{ Scavenging} = [1 - \{(A_t - A_c) / A_b\}] \times 100$$

where  $A_t$  is the absorbance of the test sample (Mel-NPs solution with DPPH),  $A_c$  is the absorbance of the control sample ( i.e. Mel-NPs solution without DPPH) and  $A_b$  is the absorbance of DPPH solution without Mel-NPs.

## 2.8. Ferric reducing action of Mel-NPs

The reducing power was measured according to the method described by Tian and Hua.<sup>48</sup> In brief, Mel-NPs (8-120 µg) were added to 400 µL of potassium ferricyanide (1%). This mixture was then incubated at 50 °C for 20 min. After incubation 400 µL of 10% trichloroacetic acid (TCA) was added and the mixture was centrifuged (Spinwin, Tarsons) at 3000 g for 10 min. 500 µL of the supernatant was mixed with 500 µL of FeCl<sub>3</sub> (0.1%) and the absorbance was measured at 700 nm. Higher absorbance indicated higher reducing power.

## 2.9. Application of Mel-NPs for enhancement of current signal in electrochemistry

### 2.9.1. Preparation of modified glassy carbon electrode

A glassy carbon electrode was cleansed by polishing it on a micro-cloth pad, using alumina powder of 1, 0.3 and 0.05 micron size in sequence. The electrode was extensively rinsed with ultrapure water after each polishing step and then allowed to dry completely at room temperature. Further, 10  $\mu\text{L}$  of PEI solution (0.01%) was loaded onto the working area of the electrode and incubated at 37  $^{\circ}\text{C}$  for 5 min. It was then washed thrice with ultrapure water. A solution of Mel-NP (10  $\mu\text{L}$ , 1  $\text{mg mL}^{-1}$ ) was then drop casted onto the working area of the PEI-functionalized electrode and dried at 37  $^{\circ}\text{C}$  for 3 h. Finally, the electrode was washed and dried completely at room temperature. This is referred as the modified electrode (GCE-PEI-Mel-NPs).

### 2.9.2. Electrochemical measurements

Cyclic voltammetric (CV) studies were carried out using CHI 1030 electrochemical workstation (CH Instruments Company, Shanghai, China). All the experiments were done in a three electrode electrochemical cell at 25  $^{\circ}\text{C}$  with GCE-PEI-Mel-NPs as the working electrode, Ag/AgCl as the reference electrode (in 3 M KCl as electrolyte) and platinum as the auxiliary electrode. The cyclic voltammetric behavior of the bare GCE and Mel-NP modified GCE were examined using  $\text{Fe}(\text{CN})_6^{4-/3-}$  (1 mM) redox couple as an electrochemical probe in PBS (0.1 M, pH 7.2). All the solutions used for the experiments were degassed by passing pure nitrogen gas for at least 10 min before use. The voltamograms were then recorded using bare GCE, PEI-GCE and Mel-NPs-PEI-GCE between the potential window of -0.2 V and +0.5 V at a scan rate of 50  $\text{mV s}^{-1}$ .

## 3. Results and discussion

### 3.1. Morphological and physico-chemical characteristics of poly(AAm-co-AGE) monolith

The monolith column of poly(AAm-co-AGE) was synthesized by polymerization of monomer units of AAm, MBAAm and AGE at optimized concentrations and sub-zero temperature. In this preparation, AAm was polymerized with MBAAm by free radical polymerization and provides

structural integrity to the monolith column. However, co-polymerized AGE provides epoxy groups on the surface of monolith column, which allows further modification of the surface for enzyme immobilization. The synthesized monolith of poly(AAm-co-AGE) was opaque and white in color (Fig. 1A), while it turned to pale yellow after amine and aldehyde surface modification (Fig. 1B). The formation of yellow color is a typical characteristic of Schiff's base formation by a reaction between the reactive amino groups of either 1,2-diaminoethane or tyrosinase enzyme and aldehyde groups of glutaraldehyde on the surface of the monolith column (Fig. 1C). In general, glutaraldehyde acts as a versatile tool in the design of biocatalyst. Considering that glutaraldehyde can be present in different forms depending on the reaction conditions, there are several possibilities by which the enzyme can bind to glutaraldehyde.<sup>49</sup> Also, our earlier study has also indicated that tyrosinase enzyme retains most of its activity when cross-linked with glutaraldehyde.<sup>31</sup>

Poly(AAm-co-AGE) monolith presented an interconnected macroporous internal architecture as observed by scanning electron microscope (Fig. 2). The diameters of pores were found to be in the range of 30-120  $\mu\text{m}$ . The water equilibrated monolith of poly(AAm-co-AGE) had soft and sponge-like property. Physical observation suggested that these monoliths were morphologically stable; however, a slight reduction in the size ( $\sim 2$  mm) was observed after complete dehydration at 37  $^{\circ}\text{C}$ . Interestingly, dried monolith returns back to their original shape within 30 s upon rehydration in aqueous medium. Poly(AAm-co-AGE) monolith presented macroporous internal architecture with the micron sized pore diameter (Table 1). Poly(AAm-co-AGE) matrix showed up to 8  $\text{mL min}^{-1}$  continuous flow of liquid through its interconnected pores. Such high flow rate could be a suitable microenvironment for the on-column biosynthesis of nanoparticles. The swelling kinetic study demonstrated that poly(AAm-co-AGE) matrix took

approximate 1 min to reach its equilibrium and showed a hydrophilic nature by high water retention capacity (swelling ratio:  $16.2 \pm 0.16$ ) (Table 1). Further, calculated hydraulic permeability of monolith was  $2.2 \times 10^{-3} \text{ m}^4 \text{ N}^{-1} \text{ s}^{-1}$  which also confirms the interconnected porous network within the monolith. Such porous architecture has already been successfully utilized for efficient separation of enzyme directly from crude cell homogenate.<sup>50</sup>

Additionally, polyacrylamide is a well known inert polymer that has already shown potential in bioprocessing.<sup>50</sup> Apart from that, the pore wall thickness (~2 to 6  $\mu\text{m}$ ) suggests that the monolith could withstand high flow. Thus, surface of poly(AAm-co-AGE) monolith offers a sturdy support for immobilization of biomolecules. Total tyrosinase enzyme bound to the column was calculated to be 8100 U by subtracting enzyme activity of unbound and washings fractions from the initial activity used. Our previous finding suggest that the process of immobilization increased the stability of tyrosinase enzyme upto 41 days with retention of 75% activity using glutaraldehyde as a crosslinker.<sup>31</sup> The rheological characterization of poly(AAm-co-AGE) monolith is described in the supplementary data (S3.1). Consequently, poly(AAm-co-AGE) monolith with amiable structural integrity and macroporous geometry was further utilized for on-column biosynthesis of Mel-NPs.

### 3.2. Biosynthesis of Mel-NPs

In our study, the immobilized enzyme was present on the surface of the monolith column, which interacted with the substrate  $L$ -Dopa and initiated the catalysis at room temperature. During circulation, molecules of  $L$ -Dopa got exposed to the immobilized enzyme under limited contact by controlling the flow of solution, which led to the formation of melanin in the form of nanoparticles. In this process, dissolved oxygen was the only source of oxygen for the oxidation reaction. Our previous study with the same enzyme showed that high oxygen concentration has a

negative impact on the enzyme activity.<sup>32</sup> The use of water as a sole solvent and the implementation of a continuous flow process based on an immobilized catalyst are both positive from the perspective of green chemistry. The biosynthesis of Mel-NPs was visually monitored by change in the color of substrate solution during the reaction (Fig. 3A). Initially, the solution of L-Dopa was colorless but as the reaction proceeded it started developing an orange color followed by light blackish color at the end of the reaction, which indicated the formation of intermediates during the synthesis of melanin.<sup>51</sup> Fig. 3B, shows the spectral changes that occur during the reaction at various time intervals. After 15 min, a strong absorbance band at 475 nm is attributed to the formation of dopachrome.<sup>31</sup> The peak at 475 nm reaches its maxima in 30 min, after which it started declining indicating the utilization of dopachrome for further synthesis. At the same time, absorbance band near 380-390 nm showed an increase which suggests the generation of indole moieties in the reaction system.<sup>52</sup> Overall, the absorbance of the solution kept on increasing with time and it was highest in the UV region. This phenomenon is possible due to the various transitions occurring in the aromatic moieties that are generated during the reaction ( $n$  to  $\pi^*$  and  $\pi$  to  $\pi^*$  transitions) and also due to the presence of complex conjugate structures formed during the reaction.<sup>53</sup> After 24 h, the solution showed broad absorbance over the entire range of UV visible spectra. There was no further change in the spectrum indicating the completion of the reaction.

### 3.3. Characterization of Mel-NPs

TEM image (Fig. 4A) showed that the Mel-NP's are spherical in shape and majority of particles were in the range of 20 to 30 nm. Table 2 draws a comparison of the size of Mel-NPs obtained through chemical as well as natural sources. Oxidation of substrates like DL-Dopa and dopamine-HCl by chemical methods produced melanin particles, in the size range from 48-490 nm.<sup>18,23-26</sup>

However, melanin obtained from natural sources such as *Sepia*<sup>18</sup> and *Ommastrephes bartrami*<sup>19</sup> were in the size range of 100-300 and 50-150 nm, respectively. In the present study, we were able to achieve particles in the size range of 20-30 nm which suggests the efficacy of our method to miniaturize the size of melanin in comparison to other approaches discussed above. Also, smaller particle size is advantageous due to higher surface area and could be of potential interest for various biological and cosmetic formulations.

Colloidal stability of the nanoparticles is one of the most important characteristics which decide the fate of the material for applications. Considering this fact, Mel-NPs were evaluated for their colloidal stability over a wide pH range. Knowledge about the electrokinetic charge present on the surface of nanomaterial can assist in understanding the complex surface phenomenon at specific pH. The electric potential between the interfacial regions of the Mel-NPs was measured at pH ranging from 2 to 11 after incubating the Mel-NPs in the respective pH solution for 8 weeks. Of all the pH's studied, Mel-NPs showed precipitation at pH 2 (Fig. 4B, inset) whereas, it showed stability at other pH. Thus, the zeta potential analysis was carried out from pH 3 to pH 11. At pH 3, Mel-NPs showed a potential of  $-15.46 \pm 0.47$  mV which decreased on increasing the pH. From pH 6 onwards, Mel-NPs showed potential near or more negative to -30 mV (Fig. 4B). These results are in the agreement with one of the thumb rule for colloidal particle stability which states that if the zeta potential is between +5 and -5 mV, the particles in the suspension are unstable due to agglomeration. However, particles show high stability when the zeta potential is around -30 mV or more negative.<sup>54</sup> Considering that most of the biological processes occur at physiological pH of 7.4, it can be presumed that the synthesized Mel-NPs will maintain the colloidal stability for biological applications.

FT-IR analysis helps in identifying the functional groups present in a compound. Fig. 5A shows the FT-IR spectra of biosynthesized Mel-NPs. The major peak position that can be assigned to Mel-NPs are at 3100-3500  $\text{cm}^{-1}$  due to the carboxylic/phenolic -O-H and -N-H stretching vibration of the indole ring, at around 1587  $\text{cm}^{-1}$  due to -COO<sup>-</sup> asymmetric stretching, -N-H bending and -C-C stretching of the aromatic ring. The peak at 1370  $\text{cm}^{-1}$  can be due to -C-N stretching vibrations, -O-H bending or -C-H rocking of alkanes. A small peak at 784  $\text{cm}^{-1}$  is due to out of plane bending vibrations of -C-H group of aromatic ring. Thus, biosynthesized Mel-NPs showed similar functional groups to that of synthetic Mel-NPs.<sup>23,55</sup>

As seen from TG graph (Fig. 5B), Mel-NPs showed good resistance against thermal degradation. Unlike other organic polymers, Mel-NPs showed a gradual weight loss on increasing the temperature. The initial weight loss of 20% till 100 °C is due to the removal of water molecules from the sample. TG analysis is in agreement with the previously reported study on melanin by Sajjan *et al.*<sup>56</sup> Biosynthesized Mel-NPs retained ~ 50% of its initial weight even after exposing to a temperature of 500 °C. This result suggests its high temperature stability which could be of use for the development of thermo-stable formulations.

### 3.4. Free radical scavenging property of Mel-NPs

There is a growing interest in natural pigments for use in food industry. Synthetic antioxidants are suspected of being toxic on prolonged use and hence attention is directed towards natural alternatives that have good antioxidant property.<sup>57</sup> Screening of natural compounds having antioxidant activity has thus been an area of focus. Since melanin is known to be present in living systems it becomes interesting to study its free radical scavenging property. The DPPH scavenging activity of Mel-NPs is shown in Fig. 6A. The scavenging activity of Mel-NPs was found to increase with increase in concentration. DPPH has a single electron and gives a purple

color in alcohol. On addition of Mel-NPs, color of the solution changed from purple to yellow, that was quantified spectrophotometrically. Mel-NPs showed  $64.5 \pm 1.1\%$  of scavenging activity at  $69.4 \mu\text{g mL}^{-1}$ , in contrast to the scavenging activity of black sesame melanin (i.e.  $47.7\%$  at  $500 \mu\text{g mL}^{-1}$ ).<sup>58</sup> Moreover, in a recent study, the melanin obtained from marine *Pseudomonas* sp.<sup>59</sup> required around 9 h for 50% scavenging of 0.1 mM DPPH solution at a concentration of  $44.7 \mu\text{g mL}^{-1}$ . However, in the present study, 50% scavenging was achieved within 20 min at a concentration of  $24 \mu\text{g mL}^{-1}$ . It is presumed that the smaller size of Mel-NPs provides a higher surface-to-volume ratio that result in increased free radical scavenging activity. The concentration of an antioxidant required to decrease the initial DPPH concentration by 50% ( $\text{IC}_{50}$ ) is a parameter that is widely used to measure the antioxidant activity.<sup>6</sup> The  $\text{IC}_{50}$  value for Mel-NP for 0.1 mM DPPH solution was calculated to be  $24 \mu\text{g mL}^{-1}$ . It was found that the  $\text{IC}_{50}$  value of Mel-NPs was lower than the natural antioxidants such as butylated hydroxytoluene (BHT) and ascorbic acid (Table 3). Ye *et al.*,<sup>61</sup> have reported that the  $\text{IC}_{50}$  values for extracellular melanin (LEM 346) and arginine modified melanin (ALEM 346) was in the range of 225-250  $\mu\text{g mL}^{-1}$ , which was 10 times higher in concentration as compared to our study. Also, a recent study has shown a higher utilization of melanin for scavenging even lower concentration of DPPH (0.05 mM)<sup>62</sup>, in comparison to present study. Thus, colloidal suspension of melanin in the form of nanoparticle could be an effective natural antioxidant for biological applications.

### 3.5. Ferric reducing action of Mel-NPs

Fig. 6B shows the ferric reducing power of Mel-NPs. In ferric reducing assay, the yellow color of the test solution changes to different shades of green, depending on the reducing power of the compound. It was observed that there was an increase in absorbance on increasing the concentration of Mel-NPs. The reducing power doubled when the concentration of Mel-NPs was

increased from 8 to 24  $\mu\text{g mL}^{-1}$ . This indicates its high reducing power and thus it can be utilized to stabilize complex biological processes.

### 3.6. Electro-catalytic application of Mel-NPs

Nanoparticles have been widely used in the field of electrochemistry to increase the sensitivity of the electrode. Owing to their small size, nanoparticles exhibit unique physical and electrochemical properties that can be used to construct new electrochemical sensors.<sup>63</sup> In electrochemistry, CV of  $\text{Fe}(\text{CN})_6^{4-/3-}$  redox couple system is widely studied as a model system. Fig. 7, shows the CV's of bare GCE along with the modified electrodes in PBS containing 1 mM  $\text{Fe}(\text{CN})_6^{4-/3-}$  as an electrochemical probe. The CV of bare GCE (Fig. 7A) shows that the redox peaks appeared at formal potential of 177 mV with a separation peak potential ( $\Delta E$ ) of about 66 mV at a scan rate of 50  $\text{mV s}^{-1}$ . However, there was no change in the voltamogram after PEI treatment which indicates that PEI did not interfere during the measurement (Fig. 7B). The high density of reactive amine groups present on PEI polymer chain work as a linker between the anionic surfaces of Mel-NPs and GCE. In addition, GCE-PEI-Mel-NPs showed an oxidation peak potential of 126 mV and a similar formal potential (176 mV) as compared to the bare GCE. Also, the peak current of the Mel-NPs modified electrode increased by 2.4 times in comparison to bare GCE (Fig. 7C). Increase in the current signal was observed after modification of the electrode with Mel-NPs, which acts as an electro-catalyst to improve the signal by enhancing electron transfer. This property can be used for increasing the sensitivity of the different electrodes which are widely used for monitoring / bio-sensing various analytes in biological samples.

#### 4. Conclusion

In summary, we have shown the synthesis of Mel-NPs by an eco-friendly approach on a porous monolith column of poly(AAm-co-AGE). The monolith column was synthesized at sub-zero temperature and its surface was eventually functionalized for immobilizing tyrosinase enzyme extracted from *A. campanulatus*. The on-column biocatalytic process allowed the transformation of L-Dopa to Mel-NPs with more precise size and shape. The interconnected macroporous architecture of the monolith column allowed unhindered flow of the Mel-NPs. The nanoparticles showed high absorption in the UV-visible region and high thermal stability. Mel-NPs showed colloidal stability at room temperature and over a wide range of pH. The bio-synthesized Mel-NPs also exhibited high free-radical scavenging and electro-catalytic activity. These results indicate the potential of biosynthesized Mel-NPs as a natural antioxidant and also for the development of electro-chemical biosensors. We anticipate that the present novel approach of synthesizing Mel-NPs will be of great interest and importance to research and industrial applications.

#### References:

1. V. V. Mody, R. Siwale, A. Singh and H. R. Mody, *J. Pharm. Bioall. Sci.*, 2010, **2**, 282-289.
2. A. Schröfel, G. Kratošová, I. Šafařík, M. Šafaříková, I. Raška and L. M. Shor, *Acta Biomater.*, 2014, **10**, 4023-4042.
3. S. Yang, D. Lu, L. Tian, F. He, G. Chen, F. Shen, H. Xu and Y. Ma, *Nanoscale*, 2011, **3**, 2261-2267.

4. R. Brayner, F. Fiévet and T. Coradin, in *Nanoparticles: A danger or promise?* ed. J. Allouche, Springer, London, UK, 2013, ch. 2, pp. 27–74.
5. D. Horn and J. Rieger, *Angew. Chem. Int. Ed.*, 2001, **40**, 4330-4361.
6. Y. Tu, Y. Sun, Y. Tian, M. Xie and J. Chen, *Food Chem.*, 2009, **114**, 1345-1350.
7. A. Kunwar, B. Adhikary, S. Jayakumar, A. Barik, S. Chattopadhyay, S. Raghukumar and K. I. Priyadarsini, *Toxicol. Appl. Pharmacol.*, 2012, **264**, 202-211.
8. A. D. Schweitzer, E. Revskaya, P. Chu, V. Pazo, M. Friedman, J. D. Nosanchuk, S. Cahill, S. Frases, A. Casadevall and E. Dadachova, *Int. J. Radiat. Oncol. Biol. Phys.*, 2010, **78**, 1494-1502.
9. V. Sava, B. Galkin, M. Y. Hong, P. C. Yang and G. S. Huang, *Food Res. Int.*, 2001, **34**, 337-343.
10. N. Mohaghehpour, N. Waleh, S. J. Garger, L. Dousman, L. K. Grill and D. Tusé, *Cell Immunol.*, 2000, **10**, 25-36.
11. L. Howells, M. Godfrey and M. J. Sauer, *Analyst*, 1994, **119**, 2691-2693.
12. D. C. Montefiori and J. Y. Zhou, *Antiviral Res.*, 1991, **15**, 11-25.
13. *US Pat.*, 5 225 45, 1993.
14. P. Meredith and T. Sarna, *Pigment Cell Res.*, 2006, **19**, 572-594.
15. M. Berggren and A. R. Dahlfors, *Adv. Mat.*, 2007, **19**, 3201-3213.
16. J. P. Bothma, J. de Boor, U. Divakar, P. E. Schwenn and P. Meredith, *Adv. Mat.*, 2008, **20**, 3539-3542.
17. C. E. Turick, A. A. Ekechukwu, C. E. Milliken, A. Casadevall and E. Dadachova, *Bioelectrochemistry*, 2011, **82**, 69-73.
18. K. Ju, Y. Lee, S. Lee, S. B. Park and J. Lee, *Biomacromolecules*, 2011, **12**, 625-632.

19. S. Chen, C. Xue, J. Wang, H. Feng, Y. Wang, Q. Ma and D. Wang, *Bioinorg. Chem. Appl.*, 2009, doi:10.1155/2009/901563.
20. R. Nicolaus, 1968. *Melanins*. Hermann Press, Paris.
21. *SU Pat.*, 939446, 1982.
22. J. C. Arnaud and P. Boré, *J. Soc. Cosmet. Chem.*, 1981, **32**, 137-152.
23. D. J. Kim, K. Ju and J. Lee, *B. Kor. Chem. Soc.*, 2012, **33**, 3788-3792.
24. M. Xiao, Y. Li, M. C. Allen, D. D. Deheyn, X. Yue, J. Zhao, N. C. Gianneschi, M. D. Shawkey and A. Dhinojwala, *ACS Nano*, 2015, **9**, 5454-5460.
25. S. Cho and S. Kim, *J. Colloid Interface Sci.*, 2015, **458**, 87-93.
26. A. Liopo, R. Su and A. A. Oravesky, *Photoacoustics*, 2015, **3**, 35-43.
27. A. G. Ingale and A. N. Chaudhari, *J. Nanomed. Nanotechnol.*, 2013, **4**, 165.
28. C. Mateo, J. M. Palomo, G. Fernandez-Lorente, J. M. Guisan and R. Fernandez-Lafuente, *Enzyme. Microb. Tech.*, 2007, **40**, 1451-1463.
29. A. S. Saini and J. S. Melo, *Bioresour. Technol.*, 2013, **149**, 155-162.
30. V. Falguera, J. Pagán and A. Ibarz, *Food Res. Int.*, 2010, **43**, 66-69.
31. A. S. Saini, J. Kumar and J. S. Melo, *Anal. Chem. Acta*, 2014, **849**, 50-56.
32. A. S. Saini and J. S. Melo, *RSC Adv.*, 2015, **5**, 47671-47680.
33. J. S. Melo and S. F. D'Souza, *Appl. Biochem. Biotechnol.*, 1992, **32**, 159-170.
34. J. J. Karimpil, J. S. Melo and S. F. D'Souza, *J. Mol. Catal. B*, 2011, **71**, 113-118.
35. J. J. Karimpil, J. S. Melo and S. F. D'Souza, *Int. J. Biol. Macromol.*, 2012, **50**, 300-302.
36. S. F. D'Souza and J. S. Melo, *Enzyme Microb. Technol.*, 1991, **13**, 508-511.
37. K. Hernandez and R. Fernandez-Lafuente, *Enzyme Microb. Technol.*, 2011, **48**, 107-122.

38. R. C. Rodrigues, C. Ortiz, Á. Berenguer-Murcia, R. Torres and R. Fernandez-Lafuente, *Chem. Soc. Rev.*, 2013, **42**, 6290-6307.
39. R. C. Rodrigues, R. C. Rodrigues and R. Fernandez-Lafuente, *Adv. Synth. Catal.*, 2011, **353**, 2216-2238.
40. J. S. Melo and S. F. D'Souza, *World J. Microb. Biot.*, 1999, **15**, 17-21.
41. C. Liu, Q. Zhang and J. Kang, *Methods Mol. Biol.*, 2013, **984**, 321-327.
42. J. S. Melo, B. S. Kubal and S. F. D'Souza, *Food Biotechnol.*, 1992, **6**, 175-186.
43. A. Tripathi, A. B. Hadapad, R. S. Hire, J. S. Melo and S. F. D'Souza, *Enzyme Microb. Technol.*, 2013, **53**, 398-405.
44. J. S. Melo, D. Sen, S. Mazumder and S. F. D'Souza, *Soft Matter*, 2013, **9**, 805-810.
45. A. Rossi, A. Morana, I. D. Lernia, A. Di-tombrino and M. DeRosa, *Ital. J. Biochem.*, 1999, **48**, 91-97.
46. P. Arvidsson, F. M. Plieva, V. I. Lozinsky, I. Y. Galaev and B. Mattiasson, *J. Chromatogr. A*, 2003, **986**, 275-290.
47. A. Tripathi, J. S. Melo and S. F. D'Souza, *J. Hazard. Mater.*, 2013, **246-247**, 87- 95.
48. B. Tian and Y. Hua, *Food Chem.*, 2005, **91**, 413-418.
49. O. Barbosa, O. Claudia, Á. Berenguer-Murica, R. Torres, R. C. Rodrigues and R. Fernández-Lafuente, *RSC Adv.*, 2014, **4**, 1583-1600.
50. A. Tripathi and A. Kumar, *Separ. Sci. Technol.*, 2012, **48**, 2410-2417.
51. J. C. García-Borrón and M. C. O. Sánchez, in *Melanins and melanosomes*, ed. J. Borovanský and P. A. Riley, Wiley-VCH, Germany, 2011, ch. 4, pp. 87-109.
52. M. Bisaglia, S. Mammi and L. Bubacco, *J. Biol. Chem.*, 2007, **282**, 15597-15605.
53. M. Magarelli, P. Passamonti and C. Renieri, *Rev. CES Med. Vet. Zootec.*, 2010, **5**, 18-28.

54. L. L. Schramm and D. G. Marangoni, in *Surfactants: Fundamentals and Applications in the Petroleum Industry*, ed. L. L. Schramm, Cambridge University Press, UK, 2009, ch. 1, pp. 3-50.
55. X. Guo, S. Chen, Y. Hu, G. Li, N. Liao, X. Ye, D. Liu and C. Xue, *J. Food Sci. Technol.*, 2013, doi: 10.1007/s13197-013-0937-7.
56. S. S. Sajjan, O. Anjaneya, G. B. Kulkarni, A. S. Nayak, S. B. Mashetty and T. B. Karegoudar, *Korean J. Microbiol. Biotechnol.*, 2013, **41**, 60-69.
57. M. Carocho and I. C. F. R. Ferreira, *Food Chem. Toxicol.*, 2013, **51**, 15-25.
58. L. Shan, L. P. Xu, Q. Z. Jin, Y. F. Liu and X. G. Wang, *J. Anhui Agriculture Sci.*, 2008, **36**, 11527-11531.
59. K. Tarangini and S. Mishra, *Res. J. Eng. Sci.*, 2013, **2**, 40-46.
60. M. Ye, Y. Wang, M. Qian, X. Chen and X. Hu, *Int. J. Basic Appl. Sci.*, 2011, **11**, 51-58.
61. M. Ye, Y. Wang, G. Guo, Y. He, Y. Lu, Y. Ye, Q. Yang and P. Yang, *Food Chem.*, 2012, **135**, 2490-2497.
62. C. G. Kumar, P. Mongolla, S. Pombala, A. KamLe and J. Joseph, *Lett. Appl. Microbiol.*, 2011, **53**, 350-358.
63. X. Luo, A. Morrin, A. J. Killard and M. R. Smyth, *Electroanalysis*, 2006, **18**, 319-326.

**Figure captions:**

**Fig.1** A setup of monolith column of poly(AAm-co-AGE) before modification (A) and after modification (B), which involve multistep surface functionalization for the immobilization of tyrosinase enzyme (C).

**Fig. 2** Scanning electron micrographs of enzyme immobilized poly(AAm-co-AGE) scaffold shows macroporous internal architecture.

**Fig.3** Color changes during the formation of Mel-NPs (A).UV-visible spectral changes during Mel-NPs synthesis (B).

**Fig. 4** TEM image (A) Zeta-potential at different pH (B) of Mel-NPs.

**Fig. 5** FT-IR spectra (A) and TG data (B) of Mel-NPs.

**Fig. 6** Percent DPPH scavenging activity (A) and ferric-reducing action (B) of Mel-NPs.

**Fig. 7** Cyclic voltamogram of (A) Bare GCE, (B) PEI-GCE and (C) Mel-NPs-PEI-GCE.

**List of tables****Table 1** Physical properties of functionalized poly(AAm-co-AGE) matrix

Properties	Functionalized poly(AAm-co-AGE) matrix
Average pore diameter	30 $\mu\text{m}$ - 120 $\mu\text{m}$
Average porosity	~ 90 %
Swelling Kinetic (equilibrium time)	~ 1 min
Swelling ratio	16.2 $\pm$ 0.16
Flow Rate	~ 8 mL min <sup>-1</sup>
Hydraulic Permeability	2.2 $\times$ 10 <sup>-3</sup> m <sup>4</sup> N <sup>-1</sup> s <sup>-1</sup>
Complex modulus (at 20 N)	
Dry	1 $\times$ 10 <sup>7</sup> Pa
Wet	6 $\times$ 10 <sup>5</sup> Pa

**Table 2** Comparison of different methods used for synthesizing nanosize melanin particles

Product	Process	Particle size
Synthetic melanin nanoparticle <sup>23</sup>	Oxidation of DL-Dopa using KMnO <sub>4</sub>	100-150 nm
Melanin like nanoparticles <sup>18</sup>	Oxidation of dopamine hydrochloride using 1 M NaOH	84 ± 16 nm
<i>Sepia eumelanin</i> <sup>18</sup>	From ink sack of cuttlefish	100-300 nm
Squid melanin <sup>19</sup>	From ink sack of <i>Ommastrephes bartrami</i>	50-150 nm
Synthetic melanin nanoparticles <sup>24</sup>	Oxidation of dopamine hydrochloride using aqueous ammonia and ethanol	146 ± 15 nm
Melanin nanospheres <sup>25</sup>	Oxidation of dopamine hydrochloride using 1M NaOH	80-490 nm
Melanin nanoparticles <sup>26</sup>	Oxidation of dopamine hydrochloride using 1 N NaOH at 60°C overnight	48 ± 12 nm
Biosynthesized Me-NP <sup>(Present study)</sup>	Oxidation of L-Dopa using tyrosianse from <i>A.campanulatus</i>	20-30 nm

**Table 3** Comparative chart of free radical scavenging property (using DPPH) of melanin and some natural antioxidants

Source	IC <sub>50</sub> (μg mL <sup>-1</sup> )	DPPH (mM)
<i>Lachnum singerianum</i> YM-292 melanin <sup>60</sup>	240	0.1
ALEM 346 and LEM 346 <sup>61</sup>	225-250	0.1
ABM ( <i>A. bridgeri</i> ) <sup>62</sup>	54.1	0.05
Synthetic melanin <sup>62</sup>	52.1	0.05
BHT <sup>60</sup>	43.4	0.1
Ascorbic acid <sup>62</sup>	40.3	0.05
Biosynthesized Me-NP <sup>(Present study)</sup>	24	0.1

List of figures

Fig. 1

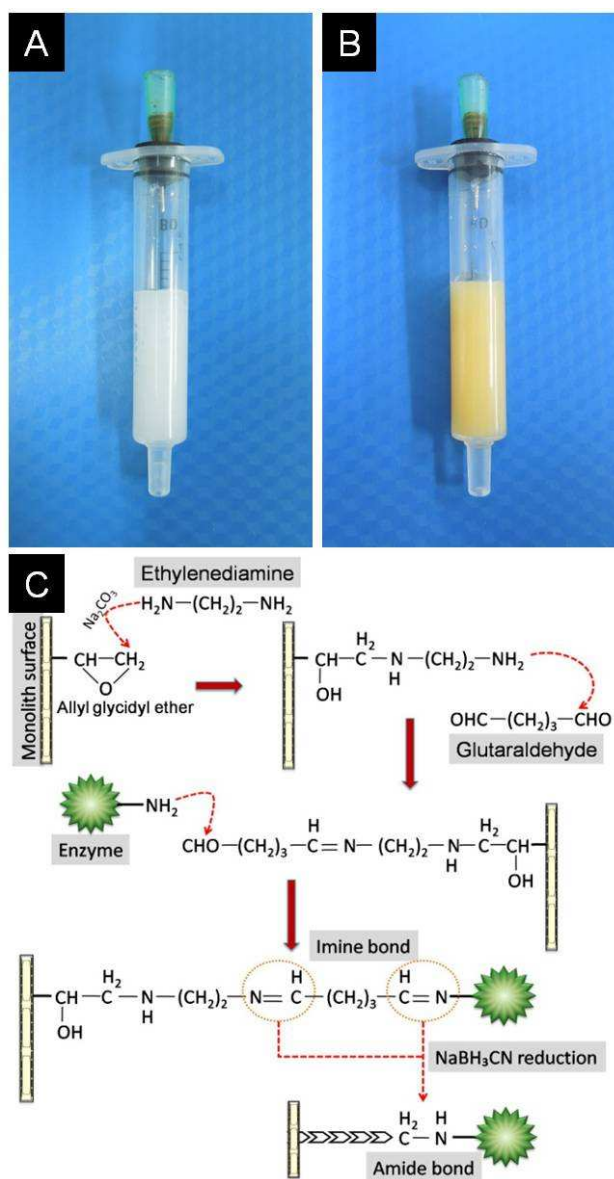


Fig. 2

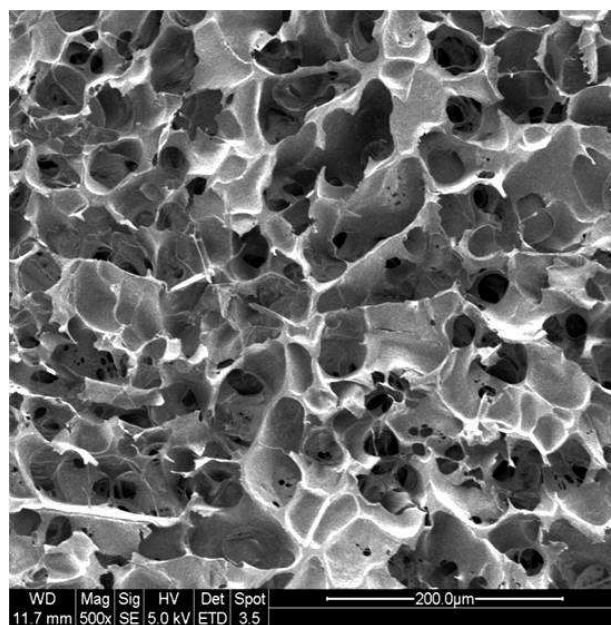


Fig.3

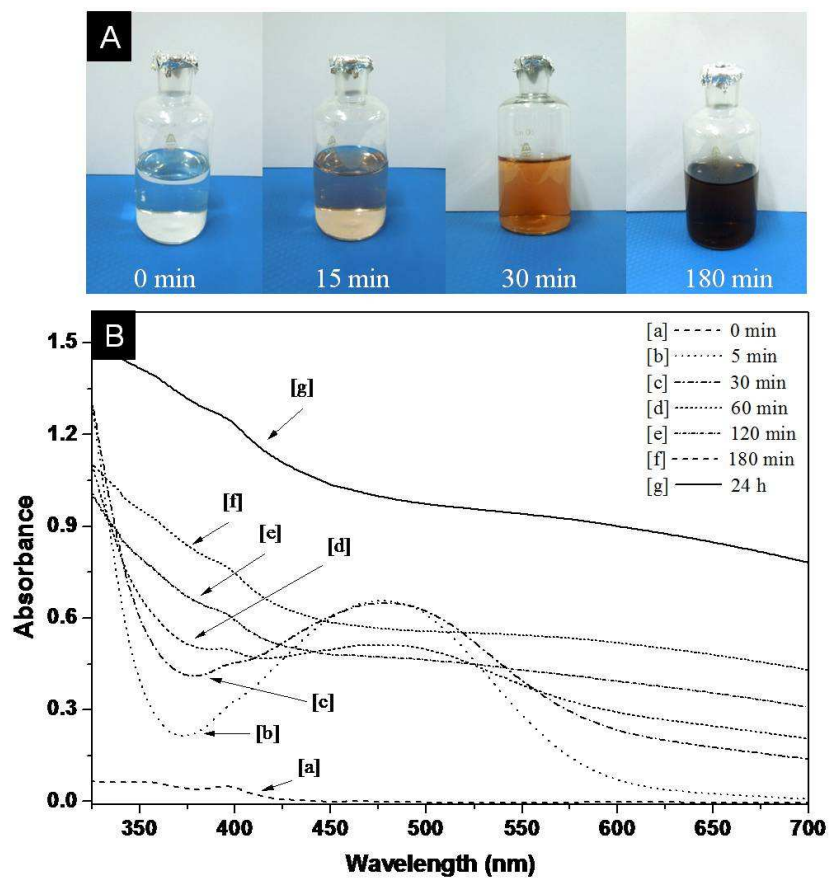


Fig. 4

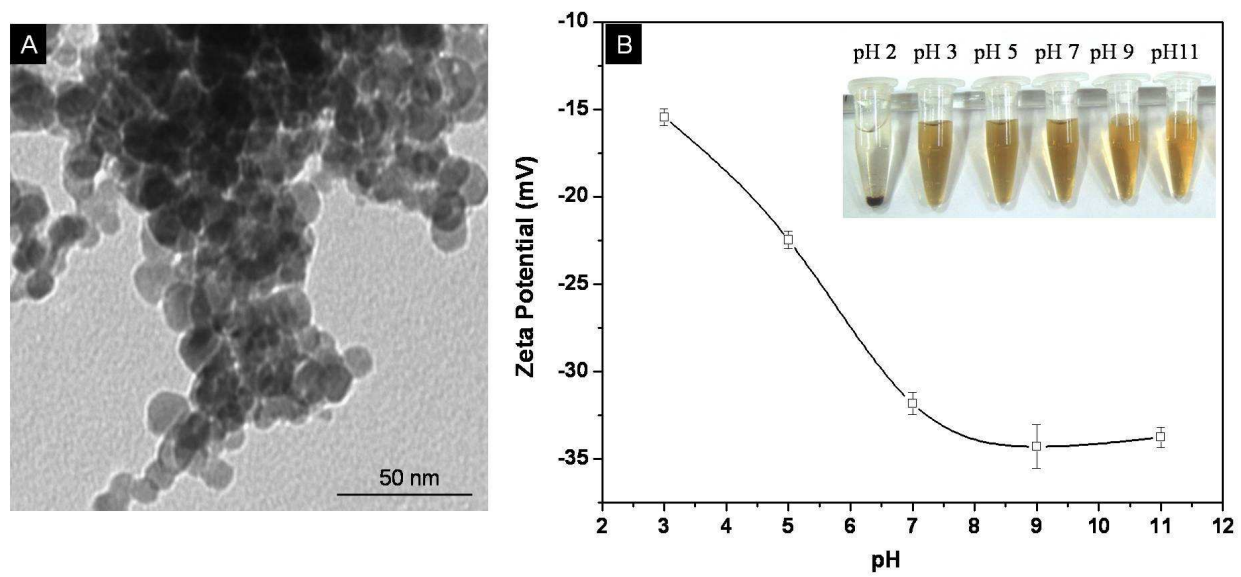


Fig. 5

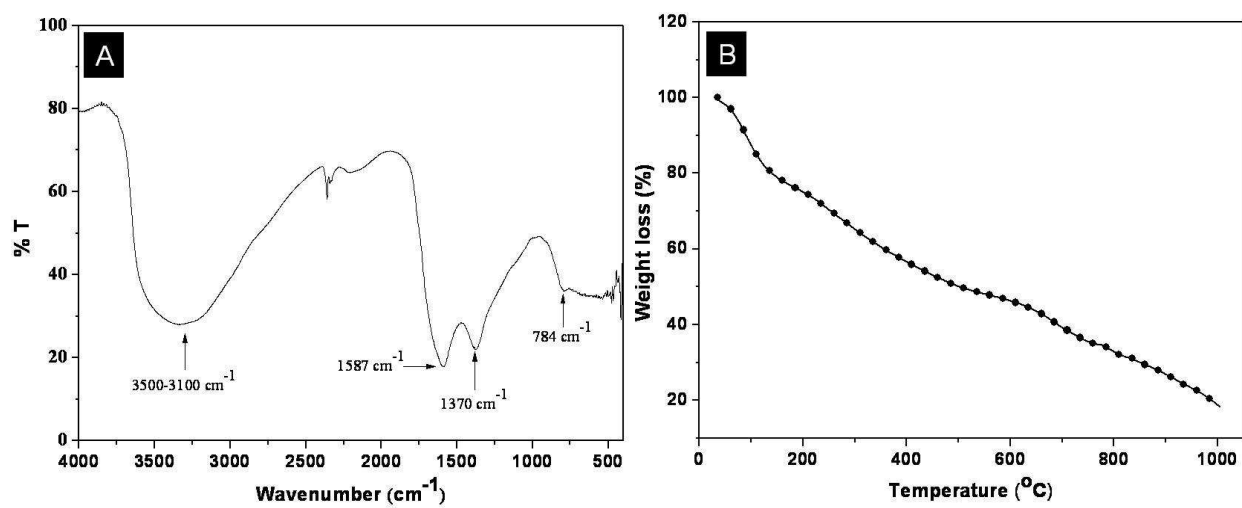


Fig. 6

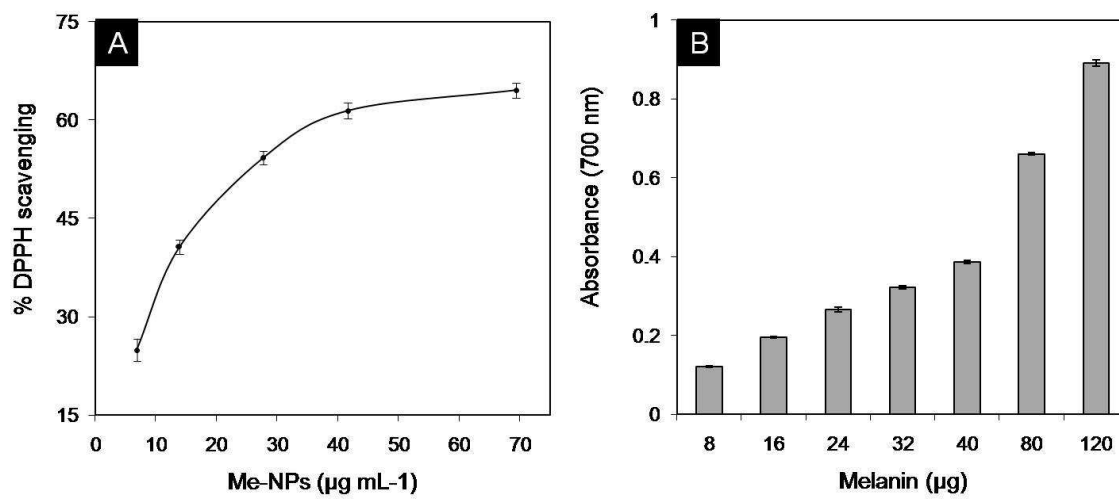


Fig. 7

